Journal Pre-proof

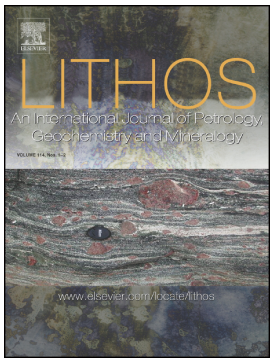

Sana Granite, a post-collisional S-type magmatic suite of the Ribeira Belt (Rio de Janeiro, SE Brazil)

Guilherme Loriato Potratz, Mauro Cesar Geraldes, Maria Virgínia Alves Martins, Bruna Saar de Almeida

PII: S0024-4937(21)00113-4

DOI: https://doi.org/10.1016/j.lithos.2021.106077

Reference: LITHOS 106077

To appear in: *LITHOS*

Received date: 20 July 2020

Revised date: 21 February 2021

Accepted date: 23 February 2021

Please cite this article as: G.L. Potratz, M.C. Geraldes, M.V.A. Martins, et al., Sana Granite, a post-collisional S-type magmatic suite of the Ribeira Belt (Rio de Janeiro, SE Brazil), *LITHOS* (2021), https://doi.org/10.1016/j.lithos.2021.106077

This is a PDF file of an article that has undergone enhancements after acceptance, such as the addition of a cover page and metadata, and formatting for readability, but it is not yet the definitive version of record. This version will undergo additional copyediting, typesetting and review before it is published in its final form, but we are providing this version to give early visibility of the article. Please note that, during the production process, errors may be discovered which could affect the content, and all legal disclaimers that apply to the journal pertain.

© 2021 Published by Elsevier.

Guilherme Loriato Potratz[1*], Mauro Cesar Geraldes[2], Maria Virgínia Alves Martins[2,4], Bruna Saar de Almeida[3]

[1] Universidade do Estado do Rio de Janeiro, Faculdade de Geologia, Programa de Pós-graduação em Análise de Bacias e Faixas Móveis, Rua São Francisco Xavier, 524, Maracanã, Rio de Janeiro, RJ, Brasil. geo.loriato@gmail.com

[2] Universidade do Estado do Rio de Janeiro, Faculdade de Geologia, Av. São Francisco Xavier, 524, sala 2020A, Maracanã. 20550-013 Rio de Janeiro, RJ, Brazil. geraldes@uerj.br, virginia.martins@ua.pt

[3] Dipartimento di Scienze della Terra, dell' Ambiente e delle Risorse. Università di Napoli Federico II. Italy. brunasaar@yahoo.com.br

[4] Universidade de Aveiro, GeoBioTec, Departamento de Geociências, Campus de Santiago, 3810-193 Aveiro, Portugal.

* Correspondent author: geo.loriato@gmail.com

Orcid:
Guilherme Loriato Potratz - https://orcid.org/0000-0003-4314-0786
Mauro Geraldes - http://orcid.org/0000-0003-2214-2814
Maria Virgínia Alves Martins - http://orcid.org/0000-0001-8348-8862
Bruna Saar de Almeida - https://orcid.org/0000-0002-2589-1669

Journal Pre-proof

ABSTRACT

The postcollisional magmatism in the Ribeira Belt, a collisional Orogen developed through several episodes during the convergence of the Pan-African/Brasiliano Orogeny, was marked in the Eastern Terrane (Rio de Janeiro, SE Brazil) by intense granitic magmatism of Cambro-Ordovician age. This magmatism was previously divided into the Suruí and Nova Friburgo suites, both interpreted as I-type granites generated by the interactions of magmas with crustal and mantle origins. This paper presents a new contribution to the understanding of the Sana Granite. It is based on the analysis of field work, mineralogical and geochemical (elemental concentrations by Inductively Coupled Plasma Emission Spectrometer, ICP-ES, and Inductively Coupled Plasma Mass Spectrometry, *ICP-MS*) data, and U-Pb dating and Lu-Hf isotope analyses, by Laser Ablation Inductively Coupled Plasma Mass Spectrometry (LA-ICP-MS) from the main body and one satellite of the Sana Granite. The results of this work show that the Sana Granite, previously grouped with the Nova Friburgo suite, presents petrographic, geochemical, and isotopic characteristics that do not match its initial petrogenetic interpretation. Data from this work show that the Sana Granite is composed of alkali feldspar

Journal Pre-proof

grani small grains ranging from fine to coarse. They are silica-supersaturated, peraluminous, and mostly alkali-calcic rocks and plot at the limit between the ferrous and magnesian fields. Crystallization ages of 480±6 million years (Ma) and 495±4 Ma are obtained in the main body of the Sana Granite, while the ages obtained in the satellite body are 506±10 Ma and 508±5 Ma. The Hf isotope data indicate crustal sources, with depleted mantle model ages (T_{DM}) varying between 2.22 and 1.69 Ga and εHf values ranging between -15.54 and -6.54. The data set from this work suggests that Sana is an S-type granite formed by the partial melting of metasedimentary rocks from the dehydration of hydrous minerals, such as biotite and muscovite. This massif is composed of muscovite-bearing peraluminous granitoids (MPGs) associated with high-pressure collisional Orogens. Considering that the characteristics of the Sana Granite are incompatible with those of the Nova Friburgo suite, it is proposed to use the Sana suite to characterize S-type granites generated in the postcollisional stage of the Ribeira Belt.

Keywords: Pan African/Brazilian Orogeny; post-collisional magmatism, MPG-type granite; zircon ages; LA-ICP-MS

1. Introduction

The Araçuaí-Ribeira Orogenic system (AROS) (Tedeschi et al., 2016) is the main geotectonic unit of the Mantiqueira Province (Almeida et al., 2000; Passarelli et al., 2019; Heilbron et al., 2020). The AROS, a simplified subdivision of the Mantiqueira Province, includes the reworked passive margin of the São Francisco paleocontinent, the internal and external arc systems and the Cabo Frio Terrane (Tedeschi et al., 2016). Aranda et al. (2020 and references herein) consider that a striking feature of the AROS is the remarkable generation of granites, which occurs in different tectonic stages (ca. 630 to 480 Ma).

The Cambro-Ordovician magmatism marks the end of the amalgamation of the Gondwana supercontinent in the segment represented by the AROS (Valeriano et al., 2011, 2016; Tupinambá et al., 2012; De Campos et al., 2016). In Rio de Janeiro state, this magmatism is represented by plutons with relatively homogeneous compositions (granites and granodiorites) and no internal deformation structures that compose the postcollisional Nova Friburgo suite (Valeriano et al., 2011; Tupinambá et al., 2012).

Liégeois et al. (1998) consider that intense interactions between mantle- and crust-derived magmas are common during the postcollisional stage of an orogenic system. In general, interactions between mantle and crust produce magmatism of varied character (bimodal), in which series with a calc-alkaline tendency and high potassium contents predominate. However, not all orogenic systems present this type of interaction, since the characteristics of postcollisional magmatism depend strongly on the evolutionary history of the orogenic system (Sylvester, 1998).

Valeriano et al. (2011) consider that the Cambro-Ordovician igneous units, free of regional deformation, located in Rio de Janeiro state, are the products of lithosphere-asthenosphere interactions during the collapse of the orogenic system after the amalgamation of the Gondwana supercontinent.

However, the main bodies of the Nova Friburgo suite do not have remarkable characteristics that corroborate intense lithosphere-asthenosphere interactions in the generation of bimodal magmatism. In the

work[illegible]arães (1999), Tupinambá (1999), Heilbron and Machado (2003) and Potratz and Valeriano (2017), the field, petrographic and geochemical characteristics presented for the Itaoca, Mangaratiba, Favela, Andorinha, Teresópolis, Nova Friburgo and Sana granites, belonging to the Nova Friburgo suite, do not demonstrate the presence of *magma* derived from the asthenosphere in the evolutionary process of these units, which leaves open interpretations about the petrogenetic process of this suite.

In the context of granitic magmatism related to the end of the collision that gave rise to AROS, as well as the collapse of this orogenic system, this work aims to answer the following questions: (a) Can Sana Granite be classified as an I-type granite, as described in previous works? (b) What is the possible source of the magmatism giving rise to Sana Granite? What are the magmatic processes involved in the genesis of Sana Granite?

2. *Geological Setting*

The Sana Granite is part of a set of igneous rocks free of regional deformation and associated with the collapse of the Araçuaí-Ribeira Orogenic system (Valeriano et al., 2011, 2016). This unit intrudes into the Coastal Domain - Eastern Terrane of the Ribeira Belt (Figure 1).

Figure 1: Location of Sana Granite in South America (A); Tectonic sketch of southeastern Brazil (B). Legend: 1 - São Francisco Craton (SFC); 2 - Brasília Belt; 3 - Paraná Basin; Ribeira Belt: 4 - Occidental Terrane; 5 - Paraíba do Sul-Embu Terrane; 6 - Oriental Terrane; 7 - Cabo Frio Terrane; 8 - Mesozoic/Tertiary alkaline intrusions. The Sana Granite location is marked with a red rectangle. Adapted from Truow et al. (2000).

Journal Pre-proof

The Araçuaí-Ribeira Orogenic system (AROS) represents the root of a deeply eroded orogen, which makes up the Mantiqueira Orogenic system (Almeida, 1977; Heilbron et al., 2004; Tedeschi et al., 2015). The origin of this orogenic system is associated with the collision of the São Francisco paleocontinent with the western part of the Angola Craton, involving other microplates amalgamated in several episodes of convergence (Heilbron et al., 2004, 2008, 2016b). The Ribeira Belt (southern region of the AROS) is limited to the north by the Araçuaí Orogen; however, this boundary is still under discussion. It is bounded to the WNW by the southern portion of the São Francisco Craton, to the SW by the southern segment of the Brasília Belt and to the south by the Luiz Alves Craton (Heilbron et al., 2016b).

The northern segment of the Ribeira Belt is divided into four tectonostratigraphic terranes, imbricated NW/W, parallel to the edge of the São Francisco Craton: Occidental Terrane, Paraíba do Sul Terrane, Oriental Terrane and Cabo Frio Terrane (Figure 1) (Truow et al., 2000; Tupinambá et al., 2007). These terranes are separated by ductile shear zones generated during the main deformation events associated with this orogenesis (Heilbron et al., 2004).

Three major prominent tectonic episodes are recorded in the southeastern region of Brazil. The first episode is recorded in the rocks of the crystalline basement and took place between the Archean and the

Journal Pre-proof

Meso São Francisco Craton rocks and the creation of the Ribeira Orogen. Finally, the third episode is associated with the breakup of the Gondwana supercontinent, generating structures related to extensional regimes. A revised tectonic model integrating new geochemical and geochronological data for the Ribeira Belt is presented in Heilbron et al. (2020).

The magmatism associated with the orogenic stages that built the Ribeira Belt (RB) developed mainly in the Oriental Terrane, which is subdivided into the Cambuci, Costeiro and Italva domains (Tupinambá et al., 2007; Heilbron et al., 2013). The Rio Negro magmatic arch represents postcollisional magmatism. The Cordeiro and Serra dos Órgãos suites correspond to syncollisional magmatism. The postcollisional and late magmatic events are represented by the Suruí and Nova Friburgo suites, respectively. Several authors (e.g., Valeriano et al., 2011, 2016; Tupinambá et al., 2012) considered that the Sana Granite should be included in the Nova Friburgo suite.

The late collisional (Suruí Suite) and postcollisional (Nova Friburgo Suite) magmatism of the RB is mostly represented by granitic bodies ranging from batholithic dimensions to stocks and veins distributed throughout Rio de Janeiro state but mainly in its central and southern regions. All these bodies are essentially composed of isotropic granitoids, generally leucocratic, with textures varying among equigranular, serial inequigranular and porphyritic (Valeriano et al., 2016). Centimetric to metric enclaves of intermediate and mafic rocks are also frequent. Lithological variations can be observed only within the units: Parati, with the occurrence of charnockites; Frade, containing quartz diorite and granodiorite; Conselheiro Paulino, with granodiorites; and São José do Ribeirão, with diorites. In units with lithological variations, macroscopic features that indicate mixing processes of magma mingling are frequent (Valeriano et al., 2011, 2016; Tupinambá et al., 2012). The Sana Granite intrudes the metasedimentary rocks of the São Fidélis Group (Supplementary Material A) that crop out in the municipalities of Casimiro de Abreu, Nova Friburgo, Macaé, Silva Jardim and Trajano de Moraes in the central-eastern region of Rio de Janeiro state.

3. Materials and Methods

Field work was carried out to recognize and describe features and to collect samples of the main body of the Sana Granite (Supplementary Material A) and one of its satellites, located southwest of the main body (Supplementary Material A). The sample locations can be observed in the map presented in Supplementary Material A. The collected samples were prepared in the Geological Laboratory for Sample Preparation of the Universidade Estado do Rio de Janeiro (LGPA-UERJ): 25 samples for whole-rock geochemical analyses; four samples for U-Pb dating; and three samples for Lu-Hf isotope analyses. In addition, 25 thin sections of this granite were obtained. The modal analysis of the rock minerals was performed manually, counting 500 points per thin section. The rock classification was based on Streckeisen (1976).

Geochemical analyses were performed at Acme Analytical Laboratories, Ltd. (Vancouver). The samples analyzed in the Inductively Coupled Plasma Emission Spectrometer (ICP-ES) instrument were opened by fusing 0.2 g of each sample with lithium metaborate/tetraborate and digesting it with diluted nitric

Journal Pre-proof

acid. MnO, Cr_2O_3, Ni and Sc concentrations. For the analyses of Ba, Be, Co, Cs, Ga, Hb, Nb, Sn, Sr, Ta, Th, U, V, W, Zr, Y and rare earth element (REE) concentrations, 0.2 g of each sample was fused with lithium metaborate/tetraborate and digestion with nitric acid, followed by Inductively Coupled Plasma Mass Spectrometry (ICP-MS) analysis. The analyses of Mo, Cu, Pb, Zn, Ni, As, Cd, Sb, Bi, Ag, Au, Hg, Tl and Se concentrations were also performed by ICP-MS after digestion of 0.5 g of each sample with aqua regia.

The dilution of the samples was accomplished by fusion, as mentioned, using robotic systems, which ensured that major oxides, refractory minerals, REEs and other highly resistant elements entered the solution. Each batch of analyzed samples contained a reagent blank, certified reference materials and 6% replicates. Analyses were performed with a Perkin Elmer Sciex ELAN 6000, 6100 or 9000 ICP-MS. Before and after each batch of samples, a set of 10 certified reference materials was run. Duplicates were analyzed for every 17 samples, and the instrument was calibrated for every 2 sample trays. The obtained data were treated and analyzed with Microsoft Excel and the Geochemical Data Toolkit (GCDkit) version 6.0 software.

The analyses to determine the U-Pb ages took place in the Multi-User Laboratory of Environment and Materials – Multilab of UERJ, using a Laser Ablation Inductively Coupled Plasma Mass Spectrometer (Thermo Neptune Plus; LA-ICP-MS). The isotopic ratios of the zircon grains were determined with multiple collectors. The analyses were carried out in the following sequence: reading a blank; reading the standard zircon GJ-1; reading nine unknown zircon grains; reading the standard zircons 91500 and GJ-1; and reading another blank. Data were transferred to Excel spreadsheets where they were treated.

In the laser ablation (LA) technique, a high-powered laser beam was used to vaporize the surface material. When coupled to the ICP-MS, this vapor was transported through a flow of helium to the plasma, where the atoms were ionized and the measurements of the isotopic ratio were provided by the spectrometer. The multicollector ICP-MS comprised nine Faraday cups and seven compact discrete dynode (CDD) ion counters. The U-Th-Pb analyses included measurements of the ^{204}Pb, ^{206}Pb, ^{207}Pb, ^{208}Pb, ^{232}Th and ^{238}U masses. Mercury represents a common contaminant in He and Ar gases. The ^{204}Hg interferes with ^{204}Pb mass counts. The ^{202}Hg, the 204 mass (^{204}Pb + ^{204}Hg), ^{206}Pb, ^{207}Pb and ^{208}Pb were detected using ion counters, while ^{238}U and ^{232}Th were measured with day-off cups. The material ablated by the laser was transported using Ar (0.80 L/min) and He (0.55 L/min) for analyses in 40 cycles for 1.045 seconds.

The zircon samples from the Sana Granite were analyzed together with international zircon standards GJ-1 (normalization data TIMS $^{207}Pb/^{206}Pb$ = 608.3 Ma, $^{206}Pb/^{238}U$ = 600.7 Ma, and $^{207}Pb/^{235}U$ = 602.2 Ma (Jackson et al., 2004) and 91500 (ID-TIMS with ages for $^{206}Pb/^{238}U$=1062.4±0.8 Ma and $^{207}Pb/^{206}Pb$=1065.4 ± 0.6 Ma), following the sequence of 1 blank, 1 standard, 9 unknown samples, 1 blank and 2 standards. The standard zircon GJ-1 for a 30 μm ablation point produced the following data: 432,000-114,000 cps of ^{206}Pb; 25,000-7,000 cps of ^{207}Pb; 6,500-4,200 cps of ^{208}Pb; 4,400-4,200 cps of ^{202}Hg; and 1,060-1,090 cps of 204 mass (^{204}Pb + ^{204}Hg). For ^{232}Th and ^{238}U measurements in Faraday cups, the values were 0.78 mV and 6.06 mV, respectively, producing an age of 603 ± 5.7 Ma. Using an Excel spreadsheet, offline corrections for the blank, Hg interference and common Pb were performed. The

Journal Pre-proof

obtai t al., 2004), aiming to calculate a conversion factor applied to all nine unknown samples. Finally, the ISOPLOT program (version 4.1.5 by Ludwing, 2012) was used to calculate ages and construct concordia diagrams.

The Lu-Hf analyses were performed with a 50 µm spot in the same locations where the U-Pb analyses were obtained. The data acquisition sequence contained 50 cycles, starting with the reading of a blank, followed by the readings of zircon standards GJ-1 and Mud Tank. After these readings, 10 grains of unknown samples were analyzed, ending with the analyses of the zircon standards 91500 and GJ-1 and one more blank reading. The analytical procedure adopted for the Lu-Hf analyses was described in detail by Alves et al. (2019).

The modeling of magmatic processes was made with PetroGram, a magmatic petrology software program based on Excel © and capable of modeling processes such as partial melting, fractional crystallization, assimilation, and mixing of magmas (Gündüz and Asan, 2021). For Sana Granite, modal and non-modal partial melting models were tested, and the most appropriate model was forward dynamic melting, in which the extracted melt is in equilibrium with the solid source up to the critical value. The equations for this type of modeling can be found in the work of Gündüz and Asan (2021). The elements Zr, Ba and Sr were used for the modeling.

4. Results

4.1 Sana Granite: Field and petrographic characteristics

The main body of the Sana Granite is a pluton of approximately 270 km^2, and its satellites occur in the form of stocks and tabular bodies that crop out to the southwest and northeast of the main body. This unit mainly outcrops in the form of flagstones on the tops of hills, in waterfalls and on slopes and occurs in the form of rolled blocks. The Sana Granite is intruded into the paragneisses of the São Fidélis Group and in syncollisional granites of the Desengano suite. The rocks are predominantly isotropic and hololeucocratic to leucocratic, with colors varying from light gray to dark gray; they have an uneven texture, with grain sizes ranging from fine to coarse (0.1 mm to 3.0 cm) (Figure 2). The rocks have a predominance of medium grains and do not show any substantial faciological variation.

This unit is composed of alkali feldspar granites, syenogranites and monzogranites (Supplementary Material B). In rare cases, microcline crystals with sizes varying from 2 to 4 cm dispersed in a fine- to medium-grained matrix are observed (Figure 2). Whitish autoliths can also be observed in the Sana Granite (Figure 2).

Figure 2 - Samples of Sana Granite with grayish color and fine to medium grains (A and B). Coarse-grained microcline crystal in the middle of a fine- to medium-grained matrix (C). Whitish autolith (D).

The mineralogical composition of the rocks is homogeneous in the pluton. These rocks have alkali feldspar, quartz, plagioclase, biotite, muscovite, allanite, zircon and opaque minerals as primary minerals.

Journal Pre-proof

Seco 3.8% alkali feldspar, 37.1% quartz, 11.2% plagioclase, 5.4% biotite, 3.5% muscovite, 1.5% allanite, 1.4% chlorite, 1.1% opaque minerals and 0.6% zircon. The modal composition of each sample is presented in Supplementary Material C.

Microcline is the main alkali feldspar. This mineral phase presents an anhydrous to subhedral granular habit (Figure 3), grain sizes ranging from 0.2 to 7.0 mm and poikilitic texture. In rare cases, graphic texture and myrmekite formation are observed. Quartz is anhedral granular and has poikilitic texture (inclusions of biotite) with grain sizes varying between 0.1 and 2.0 mm.

Plagioclase has subhedral tabular and anhedral granular habits (Figure 3) with grain sizes varying between 0.4 and 1.6 mm and sometimes changes to sericite. The biotite crystals have primarily euhedral to subhedral tabular habits (Figure 3) and secondarily form scales; both types have dimensions not exceeding 2.8 mm. Primary biotite has opaque mineral inclusions and zircons and displays chloritization, which can be partial (at the edges) or total (Figure 3).

Figure 3 - Photomicrographs of thin sections of the Sana Granite. Legend: Qtz - Quartz; Kf - K-feldspar; Pl - Plagioclase; Bt - Biotite; Ms - Muscovite; Cl - Chlorite; All - Allanite.

Similar to biotite, muscovite also occurs in primary and secondary forms (Figure 3). In its secondary form, muscovite occurs as sericite formed by feldspar alteration. Primary muscovite has tabular habits (euhedral and subhedral) (Figure 3); its dimensions can reach 3.2 mm; the edges of the crystals are well delimited, and the grains do not have inclusions.

Opaque minerals have subhedral to anhedral granular habits and grain sizes that do not exceed 2.0 mm; they are often included in or associated with biotite crystals. Allanite is granular euhedral to subhedral, with grain sizes <0.5 mm and is partially isotropized. Zircon crystals have subhedral to euhedral granular habits and grain sizes <0.1 mm and always occur as inclusions in other mineral phases, mainly in biotite.

4.2 Lithogeochemical characterization

The analyzed set of samples presents geochemical compositions similar to the modal composition. The silica contents vary between 66.81% and 74.75%, with an average value of 70.76%. The sum of the oxides varies between 98.35% and 100.8%, demonstrating that these results are within acceptable quality standards. The whole-rock geochemical results are presented in Supplementary Material D.

Figure 4 shows Harker diagrams for the major elements. Linear and polynomial curves were added in all generated diagrams through ordinary least squares regression. The best correlations are observed with the polynomial curves. However, the differences between the linear and polynomial correlation coefficients are not very significant for some oxides. Negative correlations are observed for FeO_T, MnO, MgO, CaO, TiO_2 and P_2O_5 (Figure 4).

each diagram, linear and polynomial curves were added through ordinary least squares regression.

For trace elements and REEs, the samples also demonstrate high homogeneity in composition. The analytical results for major elements and REEs are presented in Supplementary Material D. In the multielement diagram normalized to Thompson's chondrite values (1982), negative Ba, Nb, Ta, Sr, P and Ti anomalies are observed (Figure 5-A). All samples show negative europium anomalies and strong enrichments in light REEs (LREEs) relative to heavy REEs (HREEs) (Figure 5-B). This is evidenced, for instance, by the La/Yb ratios that vary between 49.4 and 267.5 (Supplementary Material D).

Figure 5 – A: Multielement diagram normalized by Thompson's chondrite values (1982). B: Diagram of rare earth elements normalized by Boynton's chondrite values (1984).

Figure 6 shows the classifications proposed by Frost et al. (2001) and Frost and Frost (2008) applied to the Sana Granite. Regarding the abundance of Fe, the samples plot in the transition between the ferrous and magnesian fields, highlighting the ferrous field. The modified alkali-calcic index (MALI) (Na_2O + K_2O – CaO; Frost et al., 2001) demonstrates that the Sana Granite is essentially alkali-calcic, with one sample in the alkaline field and 3 samples in the calc-alkaline field. In the MALI diagram, the rocks evolve relatively parallel to the fields represented in the diagram. Regarding alumina saturation, all samples are classified as peraluminous (Figure 6). The feldspathoid silica saturation index (FSSI) diagram reinforces the rocks' peraluminous character (Figure 6). In the ternary diagram by Laurent et al. (2014), used to identify magmatic sources for granitoids, the samples of Sana Granite were plotted in the field of magmas from metasedimentary rocks (Figure 7).

Figure 6: Classification diagrams for granitic rocks. Adapted from Frost et al. (2001) and Frost and Frost (2008). The red polygons indicate the Sana Granite samples, while the other plotted samples (in gray) indicate the Nova Friburgo suite's units.

Figure 7 - Discrimination diagrams of magmatic sources. Adapted from Laurent et al. (2014). The red polygons indicate the Sana Granite samples.

The dynamic melting process was modeled using the metasedimentary rocks of the Palmital Sequence, whose data are presented in the work of Capistrano et al. (2017). The samples used as a source for magmatism are essentially sillimanite-biotite gneiss interspersed with calcisilitic rocks and quartzites (Capistrano et al., 2017). Partial melting values were tested for 10%, 15%, 20%, 25%, 30%, 35%, 40% and 60% (Figure 8 - A and B). The modeling results suggest that at least 30% of partial melting were generated to form the Sana Granite.

Journal Pre-proof

Figure 8: Results of the modeling process for the dynamic melting process presented in the diagrams Zr vs Ba (A) and Sr vs Ba (B). The red curve indicates the forward dynamic melting path marking the melting proportion of the source rock (Palmital Sequence). The results show that to generate rocks similar to Sana Granite, it is necessary to have at least 30% partial melting of rocks similar to the metasedimentary rocks of the Palmital sequence.

Based on the equations presented by Boehnke et al. (2013), the estimated saturation temperatures of Zr indicate temperatures varying between 769.7°C and 900.2°C, with an average value of 825.9°C. The complete Zr saturation temperature results are presented in Supplementary Material E. As discussed later, in magmatism with high zircon inheritance, saturation temperatures mark the magmatic event's peak temperature.

4.3 U-Pb Geochronology

The dated samples were separated according to the main body (Sana 02 and Sana 10) and the satellite body (Sana 22 and Sana 28). The zircon crystals, interpreted as products of the crystallization of the Sana Granite, have similar morphology and textures (Supplementary material F). The crystals have short to long prismatic shapes, euhedral to subhedral ends and length/width ratios ranging between 2:1 and 5:1. The cathodoluminescence images demonstrate that oscillatory zoning is predominantly absent in these igneous crystals, but weak to strong oscillatory zoning can be observed in some crystals.

For analytical calculations and plotting on concordia diagrams, only data with discordance ≤5%, Th/U ratios >0.19, individual reading errors <8%, error correlation - Rho (defined as the quotient of the propagated errors of the $^{206}Pb/^{238}U$ and the $^{207}Pb/^{235}U$ ratio) >0.30 and low values of common Pb ($^{206}Pb/^{204}Pb>0.006$) were selected. The set of dated zircons in the four samples (26 in sample Sana 02, 18 in sample Sana 10, 26 in sample Sana 22, and 26 in sample Sana 28) suggests a large abundance of inherited zircons, as seen in the concordia diagrams where all analyzed samples are plotted (Figures 9 and 10). The analytical U-Th-Pb results are presented in Supplementary Material G.

In the Sana 02 sample from the main body, the ages of ten grains vary from 464±18 Ma to 492±10 Ma, with an average age of 480±6 Ma, MSWD (mean weighted standard deviation) = 0.016 and probability of 0.90 (Figure 9). The crystallization ages of the Sana 10 sample, obtained on 13 grains, vary from 485±7 Ma to 510±7 Ma, with an average age of 495±4 Ma, MSWD = 0.043 and probability of 0.84 (Figure 9).

Figure 9: Concordia diagrams with the plotted data for the Sana 02 and Sana 10 samples. In Figures A and C, all selected data from the Sana 02 and Sana 10 samples are plotted. Figures B and D show the average ages, the MSWD and the probability for the results interpreted as crystallization ages of the Sana 02 and Sana 10 samples, respectively.

Ma to 538±19 Ma, with an average age of 508±5 Ma, MSWD = 0.37 and probability = 0.55 (Figure 10). The crystallization ages in the Sana 10 sample, obtained on four grains, vary from 491±4 Ma to 518±4 Ma, with an average age of 506±10 Ma, MSWD = 0.76 and probability = 0.76 (Figure 10).

Figure 10: Concordia diagrams with the plotted data for the Sana 22 and Sana 28 samples. In Figures A and C, all selected data from the Sana 22 and Sana 28 samples are plotted, respectively. Figures B and D show the average ages, MSWD and probability for the results, interpreted as crystallization ages of the Sana 22 and Sana 28 samples, respectively.

4.4 Lu-Hf isotope geology

For the analytical Lu-Hf results, only data with error (±2SE) <1.0 and T_{DM} model ages greater than the crystallization ages of the respective samples were considered. The isotopic analyses were performed on 24 zircon crystals from the Sana 02 sample, ten zircon crystals from the Sana 22 sample and four zircon crystals from the Sana 28 sample. The εHf values vary between -15.54 and -6.54, and the T_{DM} ages vary between 2.22 and 1.69 Ga. The evolution diagram of the Hf isotope values is shown in Figure 11. The analytical results for the Lu-Hf isotope data are presented in Supplementary Material H. The analytical results for the zircon patterns analyzed in each sample are presented in Supplementary Material I, as well as the values used for the necessary corrections applied to the Lu-Hf methodology.

In addition to the isotopic results of Sana Granite, Figure 11 also show the isotopic results presented by Fernandes et al. (2015) for two samples from the São Fidélis Group, two samples from the Palmital sequence and one sample from the Buzios sequence, in which the authors identified that most of the detrimental contribution comes from Neoproterozoic sources, with Mesoproterozoic and Paleoproterozoic contributions (Figure 11).

Figure 11: Diagram of the evolution of Hf isotope data for the Sana Granite in relation to the isotope evolution of different terrestrial reservoirs: DM - depleted mantle and; CHUR - chondritic uniform reservoir. For comparison purposes, the results of isotopic analyses of the metasedimentary rocks of the Buzios and Palmital sequences, and of the São Fidelis Group, were plotted by Fernandes el al. (2015).

5. Discussion

The Sana Granite is a body intruded into the paragneiss of the São Fidélis Group and syncollisional granites of the Desengano suite. It is composed of isotropic, equigranular granitoids and has no macroscopic or microscopic deformation features. According to Valeriano et al. (2011), these characteristics allow the classification of this unit in the Nova Friburgo suite, whose origin is associated with Cambro-Ordovician magmatism, which is a product of lithosphere-asthenosphere interactions during the collapse of the Ribeira Orogen (Valeriano et al., 2011, 2016). This suite comprises the Mangaratiba,

Journal Pre-proof

José do Ribeirão, Morro do Coco and Sana units (Valeriano et al., 2011; Tupinambá et al., 2012; Valeriano et al., 2016; Potratz and Valeriano, 2017; Bione et al., 2019). Based on geochronological, compositional, and structural criteria, Valeriano et al. (2011) considered that the bodies of this suite are mainly composed of titanite, I-type, leucocratic and calc-alkaline granites.

The Sana Granite is the most different from the units belonging to the Nova Friburgo suite in terms of mineralogy and texture. Most of the bodies of the Nova Friburgo suite have significant faciological variations, mainly in rock texture. Another important aspect is the presence of intermediate to mafic rocks in most of these igneous bodies (Valeriano et al., 2011, 2016). The granite bodies of this suite that most resemble the Sana Granite are the Andorinha and Favela granites, which also do not present any faciological variation but differ slightly in their primary mineralogies (Puget and Penha, 1980; Heilbron and Machado, 2003; Valeriano et al., 2011).

Initially, considering the primary mineralogical composition, there is a problem in relation to the classification of the Sana Granite as an I-type granite (as stated by Valeriano et al., 2011); the Sana Granite is characterized by two micas (biotite and muscovite), which is a diagnostic characteristic of S-type granites, according to Chappell and White (1974, 2001). The primary nature of most Sana Granite muscovite crystals is reinforced by the textural criteria described by Miller et al. (1981). These authors considered that igneous muscovite crystals are euhedral to subhedral and have dimensions similar to the other (primary) mineral phases present in the rock. These characteristics are also observed in the analyzed unit. In addition to the textural criteria and the low degree of alteration of the Sana Granite, the lithogeochemical composition suggests that these rocks have evolved exclusively from their magmatic phase, without the presence of hydrothermal fluids. Ballouard et al. (2016) considered that concentrations of Sn <30 ppm and Cs <35 ppm and Nb/Ta ratios >5.0 in peraluminous granites indicate the absence of hydrothermal fluids in magmatic evolution. All of these criteria are met by the Sana Granite.

Another contradictory aspect related to the previous classification of the Sana Granite as an I-type granite (as stated by Valeriano et al., 2011) is its peraluminous character. Chappell and White (1974, 2001) considered that a peraluminous character is associated with S-type granites and not with I-type granites. The high potassium contents of these rocks, in addition to their structural and compositional characteristics, may have influenced Valeriano et al. (2011) to classify the Sana Granite as I-type. However, a high potassium content in a peraluminous granitoid is not a reliable indicator of the magmatic source and is not a valid criterion to differentiate I- and S-type granites since all peraluminous melts are rich in K_2O (Gao et al., 2017).

The P_2O_5 contents are directly related to the melting rate of apatite, which in turn is controlled by saturation in alumina. Gao et al. (2016) explained that a higher alumina saturation index (ASI) is related to the solubility of apatite. Therefore, I-type granites tend to have negative correlations between P_2O_5 and SiO_2 contents due to the lower apatite solubility in the source rocks. However, this observation must be taken with care, considering that an S-type granite, whose source is deficient in apatite, can also present a negative correlation between P_2O_5 and SiO_2 contents. Because the characteristics of highly differentiated granites overlap, it is difficult to classify the granitoids into types I and S, as stated by Gao et al. (2016,

and the saturation index in alumina.

Another criterion for differentiating I-type and S-type granites is the variation in the aluminous saturation index (A/CNK) in relation to increasing silica content. Clemens and Stevens (2012) highlighted that I-type granites have strong positive correlations between A/CNK indexes and SiO_2. On the other hand, Gao et al. (2016) considered that S-type granites present constant values for the A/CNK index, consistent with metasedimentary rocks. The Sana Granite has relatively constant values of the A/CNK index (Figure 12).

Figure 12 – Biplot of the A/CNK index and silica contents. The A/CNK index remains relatively constant as SiO_2 contents increase, a characteristic considered by Gao et al. (2016) as typical of S-type granites.

Answering the first question presented in this work, Sana Granite cannot be classified as an I-type granite and, therefore, cannot be inserted in the Nova Friburgo Suite since the genesis of this suite is associated with I-type granites with some mixture of magmas of mantle origin.

Considering the classification of Sana Granite as an S-type, proposed by this work, a possible source for this magmatism would be the metasedimentary rocks of the São Fidelis Group. In addition, other evidence points to metasedimentary sources, suggested such as the CaO/Na_2O ratios > 0.3, which are characteristics of magmas formed by the partial melting of metasedimentary rocks, except for psammites, as observed for example by Sylvester (1998). The ternary diagram that discriminates granitic magma sources also points to metasedimentary sources for the Sana Granite (Figure 7).

The isotopic data presented by Fernandes et al. (2015) suggest that the metasedimentary rocks of the São Fidélis Group are sources of magma for the Sana Granite. Despite some crustal contribution in its origin, the rocks of the Búzios sequence were discarded as a possible source of the Sana granite, as they present a significant juvenile contribution, as showed by the positive values of εHf (Fernandes et al., 2015). As they do not emerge in the region where the Sana granite is located, the Palmital sequence rocks possibly did not contribute as a magma source, leaving only the São Fidélis Group rocks. The São Fidélis Group is essentially composed of metapelite paragneisses with layers or lenses of other metasediments, its basal unit is represented by kinzigite gneisses, and its top unit is composed of banded gneisses, with a predominance of silimanite-biotite gneiss, and plagioclase as the primary feldspar (Heilbron et al., 2016b). Fernandes et al. (2015) interpreted the São Fidélis Group origin as immature sediments deposited close to the magmatic arc in an active margin basin.

The low Sr/Y ratios (<30) and highly variable La/Yb ratios observed in the Sana Granite (Figure 13) indicate that the partial melting that produced this granite occurred under low pressure and high temperature with significant residual plagioclase, according to Gao et al. (2016, 2017). The effect of residual plagioclase at the source is also indicated by the negative Sr, Ba and Eu anomalies. Figure 13 shows the diagram presented by Wang et al. (2016), in which the Sana Granite samples plot in the F3 field,

Journal Pre-proof

which s are compatible with the rocks of the São Fidélis Group.

Figure 13 - Discrimination of magmatic sources. A - Sr/Y ratios <30, shown in the Sr/Y vs. SiO_2 diagram; B - Variable La/Yb ratios observed in the La/Yb vs. SiO_2 diagram; C - Sr/Y vs. La/Yb diagram proposed by Wang et al. (2016) for interpretation of partial melting sources for peraluminous granitic magmas. Legend: F1 - garnet stability field with little or no plagioclase; F2 - stability field of garnet and plagioclase; F3 - plagioclase stability field with little or no garnet.

For the partial fusion process modeling, it was not possible to use data from the São Fidélis Group due to the absence of lithogeochemical data. However, the Palmital sequence is composed of the same rocks, and its genesis is similar to the São Fidélis Group (Capistrano et al., 2017). Therefore, the modeling was based on the lithogeochemical data of the Palmital sequence, presented by Capistrano et al. (2017). The values obtained in the modeling of the partial fusion process (> 30% liquid) are compatible with the results of the experiments performed by Vielzeuf and Holloway (1988) and Gardien et al. (1995), in which the referred authors obtained between 40% and 60% of liquid in melts of metapelites with muscovite and biotite at temperature around 900 ° C.

The Zr-saturation temperature obtained in this work indicates that this magmatism reached temperature similar to the experiments by Vielzeuf and Holloway (1988) and Gardien et al. (1995). The sum of total iron (FeO_T) and MgO content for the Sana Granite does not exceed 5%; therefore, this massif can be considered a product of partial melting from biotite dehydration, according to Gao et al. (2017), which confirms the hypothesis of partial fusion of biotite-rich metasedimentary protoliths. In addition, Neves (2012) considers that the high values of partial fusion obtained by Vielzeuf and Holloway (1988) and Gardien et al. (1995) can be derived from the higher proportion of plagioclase in the protoliths, implying greater fertility of the liquid. The enrichment of plagioclase in the metapelites suggested as a source of magma for the Sana Granite was described by Fernandes et al. (2015) and Capistrano et al. (2017).

Miller et al. (2013) considered that in granites rich in inherited zircons (>5%), the saturation temperature of Zr (TZr) indicates the upper limit of the magma temperature. These authors also stated that granites with high abundance of inherited zircons are formed by the partial melting of crustal rocks with limited fractionation, close to the minimum composition of albite-orthoclase-quartz, at temperatures of ≈800°C.

The mineralogical and geochemical characteristics are similar to those of MPG-type granitoids characterized by Barbarin (1996, 1999). Barbarin (1999) considered that MPG-type granites have an origin associated only with the partial melting of crustal rocks and are associated with collisional Orogens. Since there is no evidence of deformation in the Sana Granite, it can be deduced that this magmatism occurred during the postcollisional stage of the Ribeira Orogen. The Lu-Hf isotope data also support the hypothesis of an exclusively crustal contribution to the magmatism that originated the Sana Granite, demonstrated by the negative εHf values at the time of crystallization of this granite.

ation event. According to Miller et al. (2013), this is common in highly fractionated felsic melts that approach the primary composition of the separated liquid since effective melting removes all inherited and early crystallized zircons and places them in solution. In addition, the different types of zircons and the different ages obtained suggest that the magma that produced the Sana Granite should have been saturated in inherited zircons from the source rocks, which record ages of tectonic and magmatic events prior to the crystallization of the Sana Granite and may be interpreted as xenocrysts.

The concordia ages, interpreted as crystallization ages of the Sana Granite are as follows: for Sana 02 - 480±6 Ma; for Sana 10 - 495±4 Ma; for Sana 22 - 508±5 Ma; and for Sana 28 - 506±10 Ma. Despite the small differences, the main granite body is younger than its satellite. The crystallization ages obtained in this work for the main body agree with the U-Pb age of 490.9±9.8 Ma (LA-ICP-MS - zircon) obtained by Valeriano et al. (2011) for this massif. These authors cited this age as one of the criteria for placing Sana Granite in the Nova Friburgo suite.

The other obtained ages in this work can be interpreted as legacies of events preceding the magmatism that gave rise to the Sana Granite. Considering that the magma sources are the host rocks of the Sana Granite, the existence of inherited zircons is perfectly reliable since this granite intrudes the paragneiss of the São Fidélis Group. Therefore, the Sana Granite may have zircons from other tectonic-magmatic events related to the Ribeira Orogen and even to the bedrock of its precursor basin. In fact, Valeriano et al. (2011) proposed the occurrence of two main magmatic pulses for the magmatism of the postcollisional stage in the Ribeira Belt with ages of 513 Ma and 486 Ma. These authors associated the crystallization of the Sana Granite with the younger magmatic pulse. The ages obtained for the main body are in agreement with the hypothesis of two pulses of Valeriano et al. (2011). However, the ages obtained for the satellite body suggest that there were not only two magmatic pulses. In fact, this magmatism should have occurred continuously in the interval from 506±10 Ma to 480±6 Ma, at least for the formation of the Sana Granite.

Two main geodynamic models have been proposed to explain Cambro-Ordovician magmatism in the Araçuaí-Ribeira Orogenic System: the first model considers that the magmas are products of the breakdown of the subducted ocean lithosphere after continental collision (Söllner et al., 2000); the second model is related to the extensional collapse of the thickened crust during the collisional stage (Heilbron and Machado, 2003; Pedrosa-Soares et al., 2008). In both situations, it is understood that there is intense participation of the partially melted and ascending asthenospheric mantle. Considering that there is no evidence of direct interaction with magma of mantle origin in the genesis of the Sana Granite, these models of Cambro-Ordovician magmatism in the Araçuaí-Ribeira system cannot be applied to explain its formation. However, the data presented in this work for the Sana Granite indicate that its genesis was associated with the partial melting of crustal rock derived by the dehydration of minerals, such as biotite and muscovite, without significant fractionation of the primary magma.

Considering the presented information, it is suggested that the genesis of the Sana Granite is associated with the process of forward dynamic melting, whose protoliths are the metasedimentary rocks of the São Fidélis Group (Figure 14). The deposition of sediments that gave rise to the São Fidélis Group

Journal Pre-proof

shou ur the Rio Negro Magmatic Arch (Figure 14). The Cabo Frio Terrane (535 - 510 Ma) should have resulted in high-grade metamorphism of the São Fidélis Group sediments. Between the end of the collision and the collapse of the Araçuaí-Ribeira Orogenic System (AROS), the metasedimentary rocks, free of regional deformation, should have underwent partial melting, without large displacements of the generated magmas, forming the bodies of the Sana Granite (Figure 14).

The ages of 508 ± 5 Ma and 506 ± 10 Ma, obtained in one of the “satellite” bodies of the Sana Granite, suggest that the partial fusion process of the metasedimentary rocks of the São Fidélis Group began in the final collision stage of the Cabo Frio Terrane, and continued up to the collapse of AROS. This suggests that the Sana Granite is not an exclusively post-collisional unit, but it should have been originated in the interval between a late- and a post-collisional stage Also, considering that the granite in question is a product of the partial melting of metasedimentary rocks, it is suggested to remove the Sana Granite from the Nova Friburgo Suite, making it representative of a suite composed of S-type peralkaline leucogranites, called the Sana Suite.

Figure 14: Tectonic model proposed for Sana Granite. (A) Geological map with the current configuration of the Sana Granite outcrop region. Legend: Cenozoic sediments; 2 - Morro de São João (alkaline magmatism); 3 - Sana Granite; 4 - Suite Lamb; 5 - Imbé Suite; 6 - São Fidélis Group (Sillimanite-biotite gneiss); 7 - São Fidélis Group (Kinzigite); 8 - Búzios sequence; 9 - Rio Negro Complex; 10 - Trajano de Moraes Suite; 11 - Região dos Lagos Complex; 12 - Araruama Complex; 13 - Região dos Lagos Complex (metagabro). (B) Between 565 and 530 Ma, an active margin basin was filled with sediments from the São Fidélis Group and the Búzios-Palmital sequence. Legend: 14 - Rio Negro Magmatic Arch; 15 - Oriental Terrane Paleoplate; 16 - Upper Lithospheric Mantle; 17 - Immature psamite and pelites sequence (São Fidélis); 18 - Palmital Succession; 19 - Oceanic crust; 20 - Volcanic rocks and pelites (Buzios sequence); 21 - Continental crust; 22 - Passive margin. (C) Late to post-collisional stage (510 to 480 Ma) where the partial fusion of the metasedimentary rocks of the São Fidélis Group occurs and, consequently, the formation of the Sana granite. Legend: 23 - Rio Negro Magmatic Arch; 24 - Oriental Terrane Paleoplate; 25 - Upper Lithospheric Mantle; 26 - São Fidélis Group (Sillimanite-biotite gneiss); 27 - São Fidélis Group (Kinzigito); 28 - Palmital sequence; 29 - Cabo Frio Land; 30 - Sana Granite. Source: Adapted from Schmitt et al. (2008), Fernandes et al. (2015), and Heilbron et al. (2020).

6. Conclusion

The Sana granite was initially described as an I-type granite belonging to the Nova Friburgo Suite. When considering the data set presented in this work, it was observed that the Sana granite is an S-type granite, whose origin is associated with forward dynamic melting by means of the dehydration of muscovite and biotite, whose protolith is the rocks of the São Fidélis Group. The abundance of inherited zircon grains and Hf-isotopic data reinforces the essentially crustal contribution of the rocks that gave rise to the Sana Granite. The U-Pb ages indicate that the magmatic event that gave rise to this granite developed between

506± Journal Pre-proof f the Araçuaí-Ribeira Orogenic System. Therefore, the presence of a S-type granite adds another magmatic suite to the post-collisional stage of Araçuai-Ribeira Orogenic System. In addition to the Nova Friburgo and Suruí suítes, composed of I-type granites, the Sana suite is now part of the set of rocks formed at the end of the amalgamation of Gondwana supercontinent.

Declaration of conflicts of interest

The authors declare that there are no conflicts of interest.

Acknowledgements

The authors would like to thank the research promotion agencies. Guilherme Loriato Potratz would like to thank the Research Support Foundation of the Rio de Janeiro State (Fundação de Amparo à Pesquisa do Estado do Rio de Janeiro – FAPERJ; process E-26/203.112/2016) by the research grant. Mauro Geraldes would like to thank the Conselho Nacional de Desenvolvimento Científico e Tecnológico (CNPq) for the research grant (process # 301470/2016-2). Virginia Martins would like to thank the CNPq and FAPERJ for the research grants (process #302676/2019-8 and process #202.927/2019, respectively).

References

Almeida, F.F.M., 1977.O Cráton do São Francisco. Revista Brasileira de Geociências, v.7, p. 349-364.

Alves, M.I., Almeida, B.S., Cardoso, L.M.C., Santos, A.C., Appi, C., Bertotti, A.L., Chemale, F., Tavares Jr., A.D., Martins, M.V.A., Geraldes, M.C., 2019. Isotopic composition of Lu, Hf and Yb in GJ-01, 91500 and Mud Tank reference materials measured by LA-ICP-MS: application of the Lu-Hf geochronology in zircon. Journal of Sedimentary Environments 4(2), 220-248.

Aranda, R. O., Horn, A. H., Medeiros Junior, E. B. and Venturini Junior, R. 2020. Geothermobarometry of igneous rocks from Afonso Cláudio intrusive complex (Espírito Santo state, Southeastern Brazil), Araçuaí-West Congo Orogen: Further evidence for deep emplacement levels. Journal of South American Earth Sciences, 103016.

Ballouard, C., Poujol, M., Boulvais, P., Tartèse, R., Vigneresse, J.L., 2016. Nb-Ta fractionation in peraluminous granites: A marker of the magmatic-hydrothermal transition. Geology 44(3), 231-234.

Barbarin, B., 1999. A review of the relationships between granitoid types, their origins and their geodynamic environments. Lithos 46, 605-626.

Barbarin, B., 1996. Genesis of the two main types of peraluminous granitoids. Geology 24, 295-298.

Bione, F.R.A., Bongiolo, E.M., Mendes, J.C., Roland, C.L., 2019. Geochemistry, Sm-Nd isotopes and SHRIMP U-Pb geochronology of the Morro do Coco Granite (RJ, Brazil): another piece of the post-collisional magmatism of the Ribeira Belt. Brazilian Journal of Geology 49, 1-19.

Journal Pre-proof

Boeh sited. Chemical Geology 351, 324-334.

Boynton, W.V., 1984. Cosmochemistry of the rare earth elements: meteoritic studies. In: Hendersen, P. (Ed.). Rare Earth Elements Geochemistry. Elsevier, Amsterdam, pp. 63-114.

Capistrano, G.G., Schmitt, R.S., Medeiros, S.R., Fernandes, G.L.F. 2017. Evidence of a Neoproterozoic active continental margin-Geochemistry and isotope geology of high-grade paragneiss from the Ribeira Orogen, SE Brazil. Journal of South American Earth Sciences, 77, 170-184.

Chappell, B.W., White, A.J.R., 2001. Two contrasting granites types: 25 years later. Australian Journal of Earth Sciences 48, 489-499.

Chappell, B.W., 1999. Aluminiun saturation in I- and S-type granites and the characterization of fractionated haplogranites. Lithos 46, 535-551.

Chappell, B.W., White, A.J.R., 1974. Two contrasting granites types Pacific Geology, v. 8, p. 173-174.

Clemens, J.D., Stevens, G., 2012. What controls chemical variation in granitic magmas? Lithos 134-135, 317-329.

De Campos, C.P., Medeiros, S.R., Mendes, J.C., Pedrosa-Soares, A.C., Dussin, I., Ludka, I.P., Dantas, E.L. Cambro-ordovician magmatism in the Araçuaí belt (SE Brazil): snapshots from a post-collisional event J. S. Am. Earth Sci., 68 (2016), pp. 248-268.

Fernandes, G.L., Schmitt, R.S., Bongiolo, E.M., Basei, M.A.S., Mendes, J.C. Unraveling the tectonic evolution of a Neoproterozoic-Cambrian active margin in the Ribeira Orogen (SE Brazil): U-Pb and Lu-Hf provenance data. Precambrian Res., 266 (2015), pp. 337-360

Frost, B.R., Frost, C.D., 2008. A geochemical classification for feldspathic igeous rocks. Journal of Petrology 49, 1955-1969.

Frost, B.R., Arculus, R.J., Barnes, C.G., Collins, W.J., Ellis, D.J., Frost, D.C., 2001. A geochemical classification of granitic rocks. Journal of Petrology 42, 2033-2048.

Gardien, V., Thompson, A.B., Grujic, D., Ulmer, P. 1995. Experimental melting of biotite + plagioclase + quartz + muscovite assemblages and implications for crustal melting. Journal of Geophysical Research, 100(B8), 15.581-15.591.

Gao, P., Zheng, Y.F., Zao, Z.F., 2017.Triassic granites in South China: A geochemical perspective on their characteristics, petrogenesis and tectonic significance. Earth Science Reviews 173, 266-294.

Gao, P., Zheng, Y.F., Zao, Z.F., 2016. Distinction between S-type and peraluminous I-type granites: Zircon versus whole-rock geochemistry. Lithos 258-259, 77-91.

Guimarães, M.T., 1999. Geologia, petrografia, e geoquímica do Complexo Granítico de Mangaratiba - Conceição de Jacareí, RJ. MsD thesis, Universidade Federal Fluminense, UFF, 155 p. http://rigeo.cprm.gov.br/jspui/handle/doc/126.

Gündüz, M. and Asan, K. 2021. PetroGram: An excel-based petrology program for modeling of magmatic processes. Geoscience Frontiers, 12, 81-92.

Journal Pre-proof

Heilbron, M., Rodrigues, S.W.O., Ragatky, D., Silva, M.A., Monteiro, T., Freitas, N.C., Miguens, D., Girão, R., 2020.Proterozoic to Ordovician geology and tectonic evolution of Rio de Janeiro State, SE-Brazil: insights on the central Ribeira Orogen from the new 1:400,000 scale geologic map. Brazilian Journal of Geology 50, 1-25.

Heilbron, M., Eiraldo, L.G., Almeida, J.C.H., 2016a. Mapa geológico e de recursos minerais do estado do Rio de Janeiro, Escala 1:400.000. CPRM.

Heilbron, M., Eiraldo, L.G., Almeida, J.C.H., 2016b. Mapa geológico e de recursos minerais do estado do Rio de Janeiro - Nota explicativa. CPRM.

Heilbron, M., Tupinambá, M., Valeriano, C.M., Silva, L.G.E., Melo, R.S., Simonetti, A., Pedrosa-Soares, A.C., Machado, N., 2013.The Serra da Bolívia complex: the record os a new Neoproterozoic arc-related unit at Ribeira belt. Precambrian Research 238, 158-175.

Heilbron, M., Valeriano, C.M., Tassinari, C.C.G., Almeida, J., Tupinambá, M., Siga Jr, O., Truow, R.A.J., 2008. Correlation of Neoproterozoic terranes between the Ribeira Belt, SE Brazil and its African counterpart: comparative tectonic evolution and open questions. In: Pankhurst, R.J., Truow, R.A.J., Brito Neves, B.B., De Wit, M.J. (Eds), West Gondwana. Pre-Cenozoic correlations across the South Atlantic Region. Geological Society, London, Special Publications, 294, 211-237.

Heilbron, M., Pedrosa-Soares, A.C., Campos Neto, M.C., Silva, L.C., Truow, R.A.J., Janasi, V.A., 2004. Província Mantiqueira. In: Mantesso-Neto, V., Bartoreli, A., Carneiro, C.D.R., Brito-Neves, B.B. (Eds.), Geologia do Continente Sul-Americano. evolução da obra de Fernando Flávio Marques de Almeida, Beca, pp. 203-234.

Heilbron, M., Machado, N., 2003. Timing of terrane accretion in the Neoproterozoic-Eopaleozoic Ribeira Orogen (SE, Brazil). Precambrian Research 125, 87-112.

Jackson, S.E., Pearson, N.J., Griffin, W.L., Belousova, E.A. 2004. The application of laser ablation–inductively coupled plasma–mass spectrometry to in situ U–Pb zircon geochronology. Chemical Geology 211, 47-69.

Junho, M.C.B., Wiedemann, C.M., 1987. Idade, petrografia comparativa de três complexos intrusivos da província granítica do estado do Rio de Janeiro. In: Simpósio de Geologia Regional RJ/ES, Anais, pp. 120-131.

Laurent, A., Janousek, V., Magna, T., Schulmann, K., Miková, J., 2014. Petrogenesis and geochronology of a post-orogenic calc-alkaline magmatic association: the Žulová Pluton, Bohemian Massif. Journal of Geosciences, 59, 415-440.

Liégeois, J.P., Navez, J., Hertogen, J., Black, R., 1998. Contrasting origin of post-collisional high-K calc-alkaline and shoshonitic versus alkaline and peralkaline granitoids: the use of sliding normalization. Lithos, 41, 1-28.

Ludwing, K.R., 2012. User's manual for Isoplot 3.75: A geochronological toolkit for Microsoft excel. Special Publication 5. Berkeley Geochronological Center, Berkeley.

Journal Pre-proof

Mach beira belt (Brazil) and implications for the evolution of the Brazilian Orogeny. Precambrian Research 79, 347-361.

Machado, M.S., Potratz, G.L., Alves, M.I., Almeida, B.S., Tavares Jr, A.D., Nummer, A.R., Nogueira, C.C., Santos, A.C., Geraldes, M.C., 2017. SHRIMP U-Pb data of the Paleoproterozoic, Região dos Lagos Complex, Rio de Janeiro, Brazil: Implications to Ribeira Belt evolution. Journal of Sedimentary Environments, 2 (4), 301-318. https://doi.org/10.12957/jse.2017.32650

Miller, C.F., Mcdowell, S.M., MAPES, R.W., 2013. Hot and cold granites? Implications of zircon saturation temperatures and preservation of inheritance. Geology 31(6), 529-532.

Miller, C.F., Stoddard, E.F., Bradfish, L.J., Dollase, W.A., 1981.Composition of plutonic muscovite: genetic implications. Canadian Mineralogist, 19, 25-34.

Müller, D., ROCK, N.M.S., GROVES, D.I., 1992. Geochemical discrimination between shoshonitic and potassic volcanic rocks from different tectonic setting, a pilot study. Mineral Petrology 46, 259-289.

Neves, S.P. 2012. Orogenic Granites: from magmas generation to intrusion and deformation. Synergia, 148p.

Pacheco, B.T., 2010. Caracterização petrográfica e geoquímica das rochas do corpo Conselheiro Paulino (Suíte Nova Friburgo) na região Serrana do estado do Rio de Janeiro. Monografia, UERJ, 51 p.

Passarelli, C.R., Verma, S.K., McReath, I., Basei, M.A.S. and Siga Jr., O. 2019. Tracing the history from Rodinia break-up to the Gondwana amalgamation in the Embu Terrane, southern Ribeira Belt, Brazil. Lithos, 342-343, 1-17.

Pedrosa-Soares, A.C., Alkmim, F.F., Tack L., Noce, C.M., Babinski, M., Silva, L.C., Martins-Neto, M.A. 2008. Similarities and differences between the Brazilian and African counterparts of the Neoproterozoic Araçuaí-West Congo Orogen. Geological Society, Special publications, London, 249, 153-172.

Potratz, G.L., Valeriano, C.M., 2017.Petrografia e litogeoquímica do granito Itaoca, município de Campos dos Goytacazes, RJ: o representante mais jovem do magmátismo pós-colisional da Faixa Ribeira. Geonomus 25(1), 1-13.

Puget, A.J.P., Penha, H.M., 1980.Granitos da região de Ipiranga, RJ: considerações geoquímicas e petrológicas. In: Congresso Brasileiro De Geologia, Anais, 4, 2215-2230.

Schmitt, R.S., Trouw, R.A.J., Medeiros, S.R., Dantas, E.L. Age and geotectonic setting of a Late-Neoproterozoic amphibolithe and paragneiss association from southeastern Brazil based on geochemistry and Sm-Nd data. Gondwana Res., 13 (2008), pp. 502-515.

Söllner, F., Lammerer, B., Wiedemann-Leonardos, C.M. 2000. Dating the Ribeira Mobile Belt in Brazil. Zeit. Angw. Sonderheft, SH1, pp. 245-255.

Streckeisen, F., 1976. Plutonic rocks, classification and nomenclature recommended by the IUGS subcommission on the Systematics of igneous Rocks. Geotimes, pp. 26-30

Sylvester, P.J., 1998. Post-collisional strongly peraluminous granites. Lithos, [S.l.], v. 45, p. 29-44.

Journal Pre-proof

Tede s, L., Alkmim, F.F., Lana, C., Figueiredo, C., Dantas, E., Medeiros, S., De Campos, C., Corrales, F., Heilbron, M. The Ediacaran Rio Doce magmatic arc revisited (Araçuaí-Ribeira orogenic system, SE Brazil) J. S. Am. Earth Sci., 68 (2016), pp. 167-186.

Thompson, R.N., 1982. Magmatism of the British Tertiary province Scottish. Journal of Geology 18, 49-107.

Truow, R.A.J., Heilbron, M., Ribeiro, A., Paciullo, F.V.P., Valeriano, C.M., Almeida, J.C.J., Tupinambá, M., 2000. The central segment of the Ribeira Belt. In: Cordani, U., Milani, E.J. (Eds), Tectonic Evolution of South America, Rio de Janeiro, pp. 287-310.

Tupinambá, M., Teixeira, W., Heilbron, M., 2012. Evolução tectônica e magmática da Faixa Ribeira entre o Neoproterozóico e Paleozóico inferior na Região Serrana do Estado do Rio de Janeiro, Brasil. Anuário do Instituto de Geociências - UFRJ, 35, 140-151.

Tupinambá, M., Heilbron, M., Duarte, B.P., Nogueira, J.R., Valladares, C., Almeida, J., Silva, L.G.E., Medeiros, S.R., Almeida, C.G., Miranda, A., Ragatky, C.D., Mendes, J., Ludka, I., 2007. Geologia da Faixa Ribeira Setentrional: estado da arte e conexões com a Faixa Araçuaí. Geonomus 15(1), 67-79.

Tupinambá, M., 1999. Evolução tectônica e magmática da Faixa Ribeira na região Serrana do Estado do Rio de Janeiro. PhD Thesis, USP, 221 pp.

Valeriano, C.M., Mendes, J.C., Tupinambá, M., Bongiolo, E., Heilbron, M., Junho, M.C.B., 2016. Cambro-Ordovician post-collisional granites of the Ribeira Belt, SE-Brazil: A case of terminal magmatism of a hot orogen. Journal of South American Earth Sciences 68, 416-428.

Valeriano, C.M., Tupinambá, M., Simonetti, A., Heilbron, M., Almeida, J.C.H., Eiraldo, L.G., 2011. U-Pb LA-MC-ICPMS geochronology of Cambro-Ordovician post-collisional granites of the Ribeira belt, southeast Brazil: Terminal Brasiliano magmatism in central Gondwana supercontinent. Journal of South American Earth Sciences 32, 416-428.

Vielzeuf, D. and Holloway, J.R. 1988. Experimental determination of the fluid-absent melt relations in the pelite system. Contributions to Mineralogy and Petrology 98, 257-276.

Wang, Q., Hawkesworth, C.J., Wyman, D., Chung, S.L., Wu, F.Y., Li, X.H., Li, Z.X., Gou, G.N., Zhang, X.Z., Tang, G.J., Dan, W., Dong, Y.H. 2016. Pliocene-quaternary crustal melting in central and northern Tibet and insights into crustal flow. Nature Communications 7, 1-11.

Journal Pre-proof

Journal Pre-proof

Decla

☒ The authors declare that they have no known competing financial interests or personal relationships that could have appeared to influence the work reported in this paper.

☐The authors declare the following financial interests/personal relationships which may be considered as potential competing interests:

Journal Pre-proof

Journal Pre-proof

Ribeira Belt, a collisional orogen developed in the Pan African/Brasiliano Orogeny

New model for the Sana Granite (SE Brazil) formation between 506±10 MA and 480±6 MA

A S-type granite derived from the partial melting of crustal rocks at about 800ºC

Mantle heat transferred to the lithosphere produced granitic magmas on large scale

Magmatism in the transition between the late-collisional and post-collisional stage

Journal Pre-proof